Facile Fabrication of g-C₃N₄/Fe₃O₄ Photocatalyst with Enhanced Visible-Light Photocatalytic Activity towards the Degradation of Tartrazine Dye

S. Nikhil[1,] , R. Arunadevi[2], Krishna Veni[3], C. Sudhakar[1], A. Karthika[4], A. Suganthi[4,*] and M. Rajarajan[5,*,]

[1]School of Chemistry, Madurai Kamaraj University, Madurai-625021, India
[2]P.G. & Research Department of Chemistry, D.K.M. College for Women, Vellore-632001, India
[3]P.G. & Research Department of Chemistry, C.P.A. College, Bodinayakanur-625582, India
[4]P.G. & Research Department of Chemistry, Thiagarajar College, Madurai-625009, India
[5]Directorate of Distance Education, Madurai Kamaraj University, Madurai-625021, India

*Corresponding authors: E-mail: rajarajanchem1962@gmail.com; suganthiphd09@gmail.com

The removal of tartrazine dye from aqueous solution using g-C₃N₄/Fe₃O₄ nanocomposites was studied. The g-C₃N₄/Fe₃O₄ nanocomposites were synthesized using simple co-precipitation method. The synthesized nanocomposites were characterized by spectral (UV-Vis DRS, FT-IR) and analytical (PXRD, SEM, EDAX, HRTEM) techniques. Photodegradation of tartrazine dye using the synthesized catalyst was studied. The g-C₃N₄/Fe₃O₄ nanocomposites exhibited excellent photocatalytic performance by degrading tartrazine (90%) at 0.1 g/L of catalyst and 20 μM initial dye concentration at pH 3. The excellent performance by the catalyst was attributed to the highest electron hole pair generation. The kinetic study revealed that the photodegradation of tartrazine obeyed pseudo first-order kinetics.

Keywords: g-C₃N₄/Fe₃O₄ nanocomposites, Tartrazine degradation, Photocatalyst, Electron-hole pair, Pseudo first order kinetics.

INTRODUCTION

Environmental pollution is one of the major problems being faced by the 21st century world. Among the various pollutions, contamination of water resources possess a serious threat to the mankind. Dyes which appear in the effluents left from various textile, leather, food processing, paper and dye manufacturing industries play a major role in polluting the water resources around the globe. These coloured effluents not only create environmental hazards but also forms a major threat to aquatic and human life. For example, reports are there about azo and nitro compounds been reduced in sediments of aquatic bodies, which form carcinogenic amines [1-9].

Tartrazine is a yellow dye used in cosmetics, medicines, soft drinks, puddings, ice cream, candy and other numerous food items. Tartrazine is used instead of β-carotine since, it achieves similar colour as well as cheaper than β-carotine. Tartrazine can induce asthma, behavioural abnormalities, thyroid cancer, migrane, *etc*. Besides its water soluble nature accelerates the contamination of water bodies since, it constitutes a

major part in industrial effluents discharged into water bodies [1,10-12]. Conventional methods like biological treatment, chemical oxidation, physical adsorption, membrane separation [13,14]are applied for the degradation of pollutants. Nevertheless these methods have shortcomings such as low efficiency, incomplete degradation, which leads to the secondary pollution, limited scope of use, high energy consumption [15]. In this context, the relevance of advanced oxidation processes comes to play.

Advanced oxidation processes (AOP) are environment friendly techniques which can remove a wide range of pollutants in air, water, petroleum hydrocarbons, pesticides and so [16]. AOPs generate reactive oxygen species like hydroxyl radicals with one unpaired electron, which possess shorter life time. This makes them to react rapidly with various chemical species which are difficult to degrade. And this forms thermodynamically stable oxidation products such as carbon dioxide, water and other biodegradable organics [17-19]. Photocatalysis is a key route to degrade organic pollutants, which are difficult to decompose to benign components. Efficiency of photocatalyst

depends on its ability to generate electron-hole pairs, which can create free radicals to react with dyes and other organic pollutants [20-22].

Semiconductor materials are extensively used as photocatalysts to degrade organic pollutants under visible light irradiation. Their excellent charge transfer ability makes them a promising candidate for photocatalytic applications [23-25]. Nevertheless fast recombination of photogenerated electron-hole pairs, reduced electrical conductivity, poor visible light response, *etc.* are some challenges for these materials [26,27]. This can be overcome by selected modifications on these semiconductor catalysts and improve their performance. Graphitic carbon nitride (g-C_3N_4) is an n-type metal free polymeric semiconductor with a unique 2D structure with band gap 2.6-2.7 eV [28]. Pure g-C_3N_4 possess rapid recombination of photogenerated electron-hole pairs, lowered electrical conductivity, deprived visible light response, *etc.* But incorporation with various nanomaterials like metal oxides, carbon materials, *etc.* can reduce the electron-hole recombination rates and thereby improve its efficiency as photocatalyst [29-31].

In present work, the g-C_3N_4/Fe_3O_4 nanocomposites were synthesized using simple co-precipitation method and characterized by various spectroscopic, analytical and morphological techniques. Photocatalytic applications of the synthesized nanocomposite was evaluated by taking tartrazine as the model dye and the obtained results were compared with other photocatalysts and found that synthesized catalyst exhibit excellent catalytic activity.

EXPERIMENTAL

Thiourea, ferric chloride, hydrochloric acid and sodium hydroxide were purchased from Merck Co., USA. The chemicals were of analytical grade and used without further purification. Double distilled water was used throughout the experiment.

Synthesis of g-C_3N_4: The graphitic carbon nitride was synthesized by calcination of thiourea. Thiourea (10 g) was added in to a semi-closed alumina crucible and heated to 550 °C at a heating rate of 15 °C min^{-1} in a muffle furnace for 2 h. Followed by the reaction, alumina crucible was cooled to room temperature. The resulted bulk g-C_3N_4 was collected and grounded in to powder.

Synthesis of Fe_3O_4: The Fe_3O_4 nanoparticles were synthesized by following the simple co-precipitation method. Initially, 5 g of $FeCl_3$ was dissolved in 100 mL diluted HCl followed by continuous stirring. The NaOH solution was added until complete precipitation (solution pH value 5-8) was obtained. After stirring for another 3 h, the precipitate was filtered and washed thoroughly with distilled water. Finally, the precipate was dired at 100 °C for 1 h and calcinated at 450 °C for 3 h to obtain Fe_3O_4 nanoparticles.

Synthesis of g-C_3N_4/Fe_3O_4 nanocomposite: The g-C_3N_4-Fe_3O_4 nanocomposite have been synthesized by following the simple co-precipitation method. The Fe_3O_4 (4.7890 g) and g-C_3N_4 (0.9768 g) were dissolved in 20 mL of ethanol. The obtained mixture was sonicated for 0.5 h and followed by stirring for 3 h. The attained precipitate was filtered, washed with ethanol and double distilled water for several times. Further, it was dried at 100 °C in hot air oven for 1 h followed by calcination at 450 °C for 3 h to obtain finely powdered g-C_3N_4/Fe_3O_4 nanocomposite.

Characterization: The structure and phase details of the samples were determined by X-ray powder diffraction with Cu$K\alpha$ radiation at 25 °C using XPERT PRO. Functional group analysis of synthesized samples were carried out by Bruker TENSOR II ATR FTIR in the range 4000 to 400 cm^{-1} with a resolution of 4 cm^{-1} (IR Affinity-1) using KBr-nanocomposite mixture in the form of pellets.

The UV-Vis diffuse reflectance spectral measurements for dry-pressed disk samples were carried out in a JASCOV-550 double beam spectrophotometer with PMT detector equipped with an integrating sphere assembly, using $BaSO_4$ as a reference sample. The spectrum was recorded at room temperature in the wavelength range from 200 nm to 800 nm. The surface morphology was analyzed by scanning electron microscopy using JM 6701F-6701 instrument in both secondary and backscattered electron modes. The elemental analysis was conducted by an energy dispersive X-ray spectroscopy (EDX) attached to the (SEM).

Photocatalytic measurements: The photocatalytic activities of the as-synthesized samples were evaluated by the degradation of tartrazine under visible light irradiation. Photocatalytic experiments were carried out in an immersion type photoreactor. Tartrazine (300 mL) with certain amount of photocatalyst was taken in a cylindrical glass vessel, which was surrounded by a circulating water jacket to cool the lamp. Air was bubbled continuously into the aliquot by an air bump in order to provide a constant source of dissolved oxygen. Before light irradiation, the reaction mixture was stirred in dark for 0.5 h to achieve the adsorption-desorption equilibrium between the catalyst and the dye molecules. The simulated solar light irradiation was produced by a 300 W Xenon arc lamp. Aliquot (5 mL) was collected at regular time interval of 30 min during the course of light irradiation. The samples were centrifuged in order to remove the photocatalyst and the filtrate was analyzed by UV-visible spectrometer at λ_{max} = 425 nm to calculate the residual methylene blue concentration. The photodegradation of tartrazine was calculated as follows:

$$\text{Photodegradation (\%)} = \frac{C_o - C}{C_o} \times 100$$

where, C_o = concentration of phenol before irradiation time; C = concentration of phenol after a certain irradiation time.

RESULTS AND DISCUSSION

PXRD analysis: The crystal structures of Fe_3O_4, g-C_3N_4 and g-C_3N_4/Fe_3O_4 nanocomposites were analyzed by X-ray diffraction. A weak peak at 11.8° and other strong peak at 27.5° obtained for g-C_3N_4 correspond to (100) and (002) planes, which attributes to the in-plane structural arrangement of tri-*s*-triazine units and the interplanar stacking of the conjugated aromatic systems, respectively. The structure of synthesized nanoparticles is cubic face centered according to the JCPDS value of g-C_3N_4 which is 87-1526 [32]. It can be seen that there is a series of

very broad diffraction peaks in XRD pattern for Fe_3O_4 nanoparticles. Fig. 1a-c displays XRD patterns of g-C_3N_4, Fe_3O_4, g-C_3N_4/Fe_3O_4, where the peaks of Fe_3O_4 crystal phase at 2θ = 30.8º, 33.34º, 35.89º, 43.64º, 53.2º, 55.9º [33].
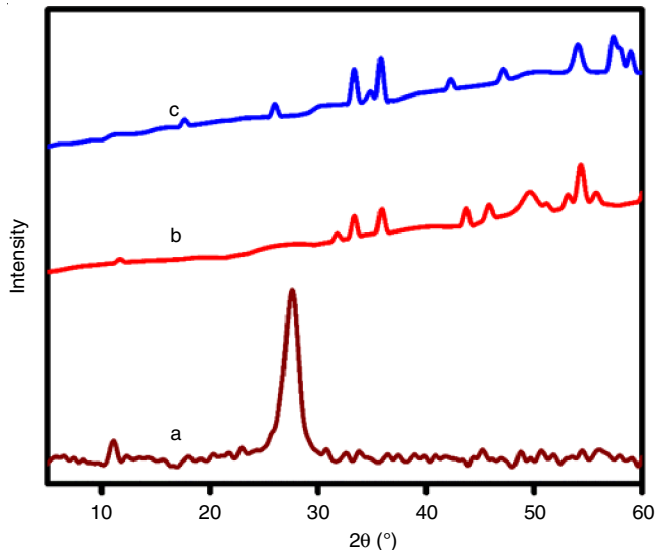
Fig. 1.   XRD image of (a) g-C_3N_4, (b) Fe_3O_4 and (c) g-C_3N_4/Fe_3O_4 nanocomposites

Fig. 2.   FT-IR spectra of (a) g-C_3N_4, (b) Fe_3O_4 and (c) g-C_3N_4/Fe_3O_4 nanocomposites

FT IR studies: The FT-IR spectra of pure g-C_3N_4, pure Fe_3O_4 and g-C_3N_4-Fe_3O_4 hybrid nanocomposites are shown in Fig. 2. In FT-IR spectrum of g-C_3N_4 (Fig. 2a), the broad band between 3000 and 3300 cm^{-1} is indicative of the N-H stretching vibrations and of O-H stretching vibrations of the physically absorbed water molecules. Strong bands observed between 1400 and 1700 cm^{-1} are attributed to C≡N heterocycles. Another characteristic peak at around 800 cm^{-1} corresponds to the triazine units in g-C_3N_4 [34]. The strong Fe-O band between 550 and 600 cm^{-1} is clearly visible at pure Fe_3O_4 [35] (Fig. 2b) and the g-C_3N_4-Fe_3O_4 hybrid nanocomposites (Fig. 2c). But the charac-
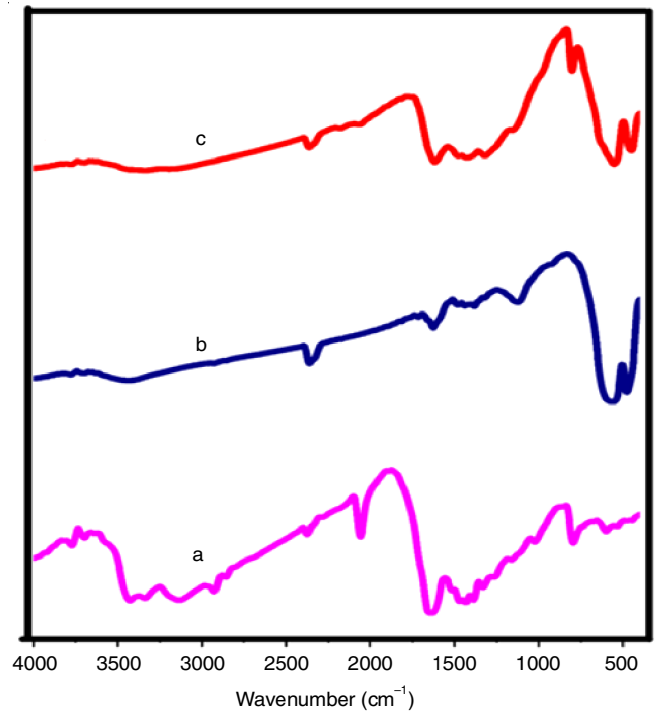
teristic peaks for g-C_3N_4 are absent or diminished in the compound suggests the reduction of g-C_3N_4.

UV-vis-DRS studies: The UV-vis DRS of pure g-C_3N_4, Fe_3O_4 and g-C_3N_4/Fe_3O_4 nanocomposites are shown in Fig. 3. It shows a sharp edge in the absorption intensity of pure g-C_3N_4 at 430 nm [36]. The figure also shows that g-C_3N_4/Fe_3O_4 nanocomposites displays the more intense visible light absorption ability with a significant red shift which is resulted from the junction formation of pure g-C_3N_4 with the Fe_3O_4 with narrower band gap. And the results also shows that more photo induced charges were generated when the nanocomposite was excited
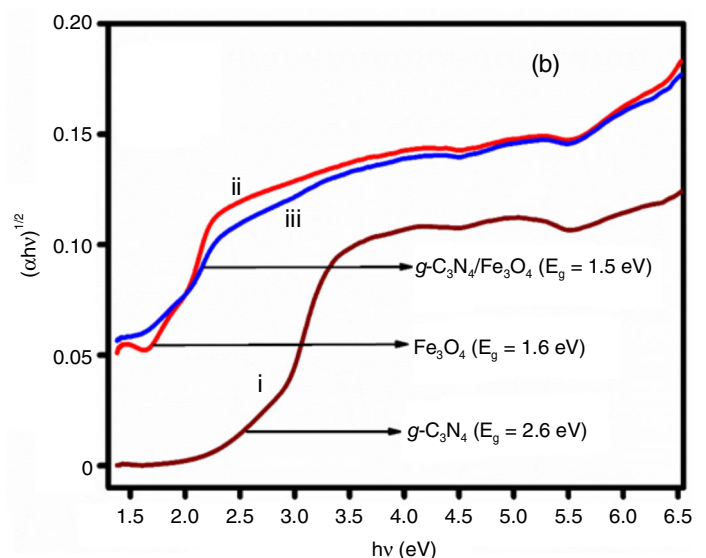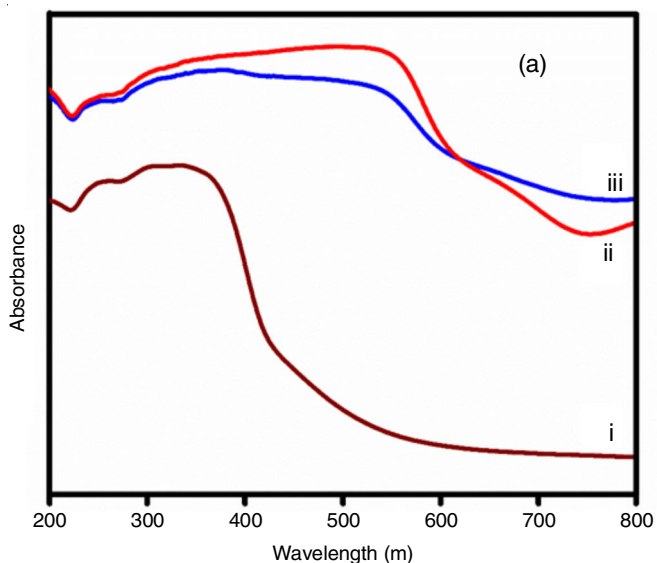

Fig. 3.   UV-Vis-DRS spectrum of i) g-C_3N_4, ii) Fe_3O_4 and iii) g-C_3N_4/Fe_3O_4 nanocomposites (a) and Tauc plots of (i) g-C_3N_4 (ii) Fe_3O_4, (iii) g-C_3N_4/Fe_3O_4 nanocomposites (b)

under visible light irradiation and resulted in superior photocatalytic performance [37].

$$(\alpha h\nu)^{1/\gamma} = B(h\nu - E_g) \qquad (2)$$

where h = planck constant, α = absorption coefficient, ν = photon's frequency, E_g = band gap energy and B = proportionality constant, respectively. The value of γ depends on the transition and is ½ for direct and 2 for indirect transition band gaps [38]. The E_g values were estimated by extrapolation of the linear part of the curves obtained by plotting $(\alpha h\nu)^2$ *versus* hν. The E_g values of the samples obtained are between about 2.6 eV, 1.6 eV and 1.5 eV for pure g-C_3N_4, Fe_3O_4 and g-C_3N_4/Fe_3O_4 nanocomposites, respectively.

SEM and EDX studies: Morphology of the as-prepared samples was investigated using SEM analysis and the results are shown in Fig. 4. The as-prepared g-C_3N_4 and Fe_3O_4 nanoparticles exhibit flakes and agglomerated sphere structures (Fig. 4a-b). The SEM image of g-C_3N_4/Fe_3O_4 nanocomposite shows deposition of the Fe_3O_4 on g-C_3N_4 indicated by the flakes with sphere like morphology (Fig. 4c). The EDX spectra also recorded to confirm purity of g-C_3N_4, Fe_3O_4 and g-C_3N_4/Fe_3O_4 nanocomposites and the result are given in Fig. 4d. It can be seen clearly that the existence of C and N elements in g-C_3N_4 and C, N, Fe and O elements in g-C_3N_4/Fe_3O_4 nanocomposites. Weight percentages for different compounds and elements in

g-C_3N_4/Fe_3O_4 nanocomposite were calculated and are shown in Table-1. It is evident that these values are similar to the theoretical compositions.

TABLE-1 EDAX DATA OF g-C_3N_4, Fe_3O_4 AND g-C_3N_4/Fe_3O_4 NANOCOMPOSITES			
Element	Weight (%)	Weight (%) Sigma	Atomic (%)
C	20.51	1.30	30.95
N	19.41	2.46	25.12
O	30.23	1.33	34.25
Fe	29.85	1.12	9.69

HRTEM studies: The high resolution transmission electron microscopy analysis was carried out for g-C_3N_4/Fe_3O_4 nanocomposites and the images are shown in Fig. 5. The results indicates that g-C_3N_4/Fe_3O_4 sample exhibited good crystalline and clear lattice fringes. Fe_3O_4 nanoparticles are tend to be close and connected to each other. After introducing Fe_3O_4, amounts of nanoparticles are mussily accumulated on the surface of g-C_3N_4 nanosheets, resulting in the formation of a heterostructure. From the enlarge image of g-C_3N_4/Fe_3O_4 nanocomposites two phases of g-C_3N_4 (light part) and Fe_3O_4 (dark part) are clearly observed and closely in contact to form an intimate interface, which further demonstrates that Fe_3O_4 nanoparticles have well covered the surface of g-C_3N_4.
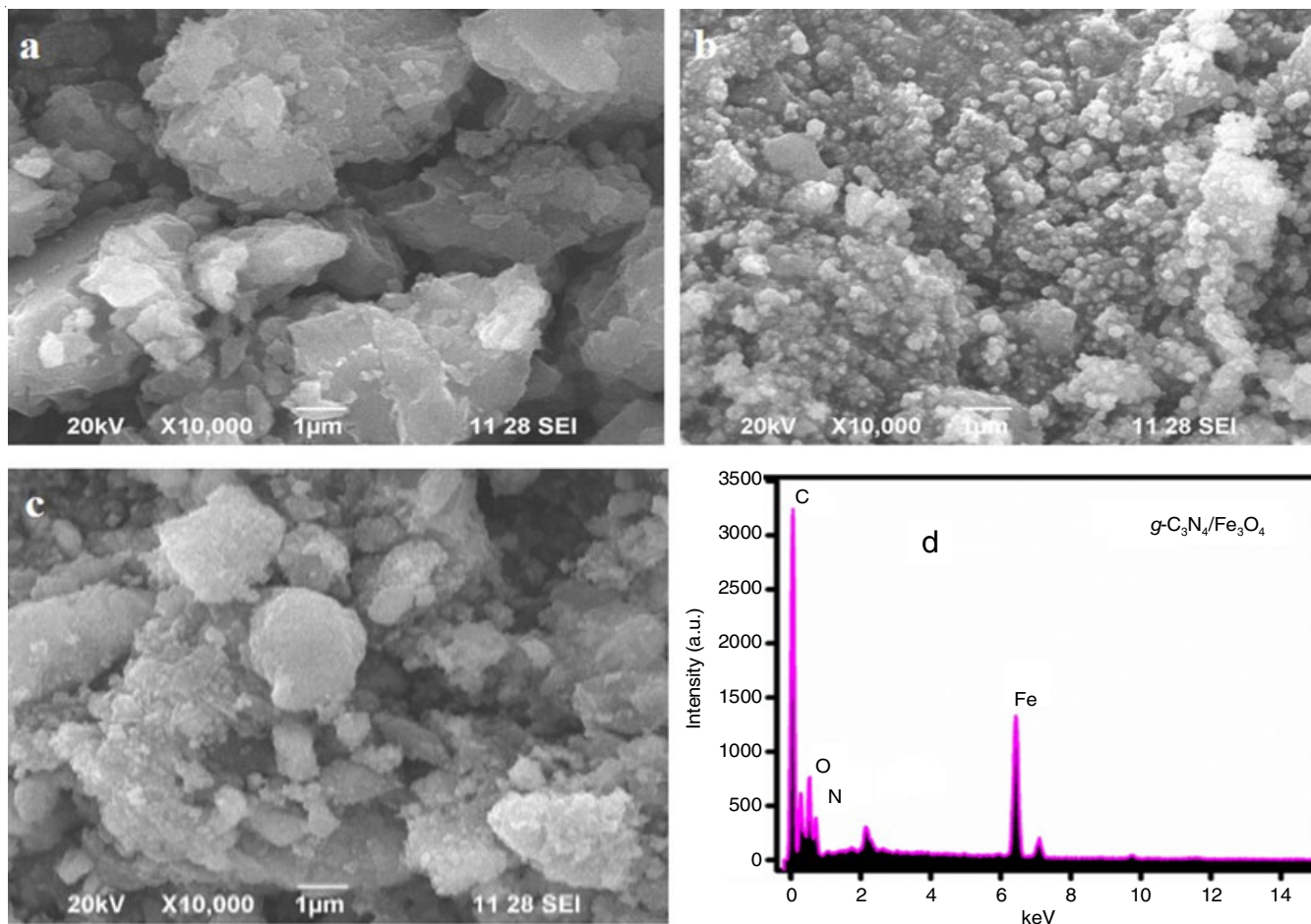

Fig. 4. SEM images of (a) g-C_3N_4 (b) Fe_3O_4 (c) g-C_3N_4/Fe_3O_4 nanocomposites (d) EDX image of g-C_3N_4/Fe_3O_4
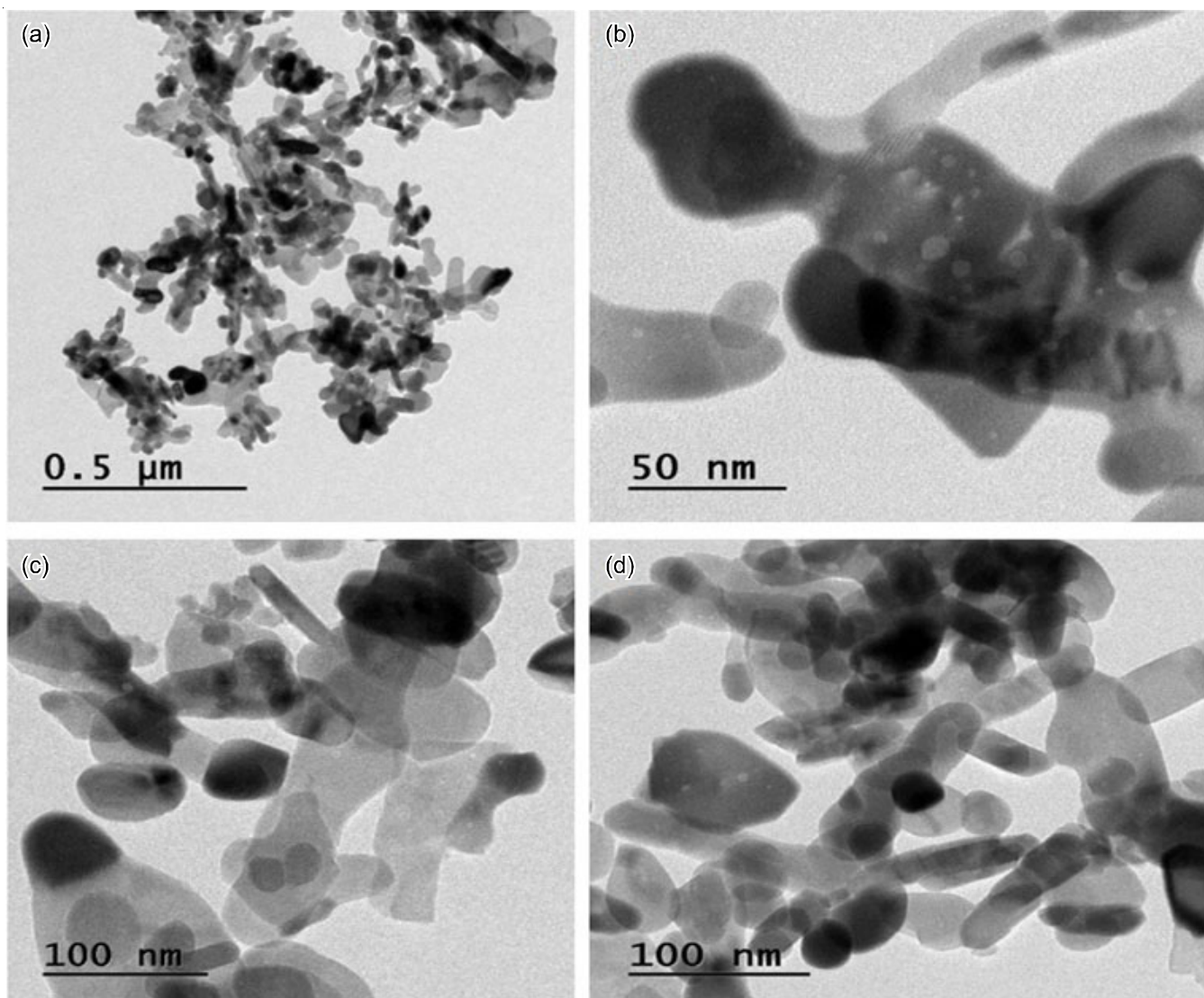
Fig. 5. HRTEM images of g-C$_3$N$_4$/Fe$_3$O$_4$ nanocomposites

Photocatalytic activity

Photodegradation of tartrazine: The photocatalytic performance of the prepared nanoparticle (0.15 g/L) was investigated by the degradation of tartrazine (20 μM) under visible light irradiation. The photodegradation was monitored by recording the absorbance of tartrazine (λ_{max} = 425 nm) as a function of irradiation time. Fig. 6a shows the deviations in absorption spectra of tartrazine using g-C$_3$N$_4$-Fe$_3$O$_4$ at various time intervals. It was noticed that the absorption intensity of tartrazine decreases gradually with time and this indicates the degradation of dye on the surface of g-C$_3$N$_4$-Fe$_3$O$_4$. The plot of variations in tartrazine concentration (C/C$_0$) against reaction time for different catalysts are presented in Fig. 6b. This shows that the tartrazine does not significantly degrade in the presence of the photocatalyst without visible light treatment. Also, there is no substantial degradation in the absence of photocatalyst under light irradiation, which indicates the dye is resistant to self-photolysis in aqueous medium under light irradiation. The g-C$_3$N$_4$-Fe$_3$O$_4$ composites showed better photocatalytic activity (90%) than pure g-C$_3$N$_4$ and Fe$_3$O$_4$ indicating that g-C$_3$N$_4$ doping

on Fe$_3$O$_4$ played an important role in the enhancement of photocatalytic activity [39,40].

Photodecolorization kinetics of tartrazine: The kinetics of photodecolorization of tartrazine was studied by conducting the experiments under optimum conditions. In all experiments, the decolorization followed pseudo first order kinetics (plots of -ln (C/C$_0$) *vs.* time showed linear relationship).

$$-\ln\left(\frac{C}{C_o}\right) = kt \qquad (3)$$

where C = concentration of tartrazine remaining in the solution at irradiation time t; C$_o$ = initial concentration at t = 0. First order rate constant was evaluated from the slope of -ln (C/C$_0$) *vs.* time plots shown in Fig. 7.

Mechanism of tartrazine degradation by g-C$_3$N$_4$-Fe$_3$O$_4$: The following mechanism can be proposed for the solar-light driven photodegradation of tartrazine using g-C$_3$N$_4$/Fe$_3$O$_4$ nanocomposites as shown in Fig. 8. When the photocatalyst is irradiated by visible light, electron-hole pair generates in Fe$_3$O$_4$ (narrow band gap semiconductor) and the photogenerated
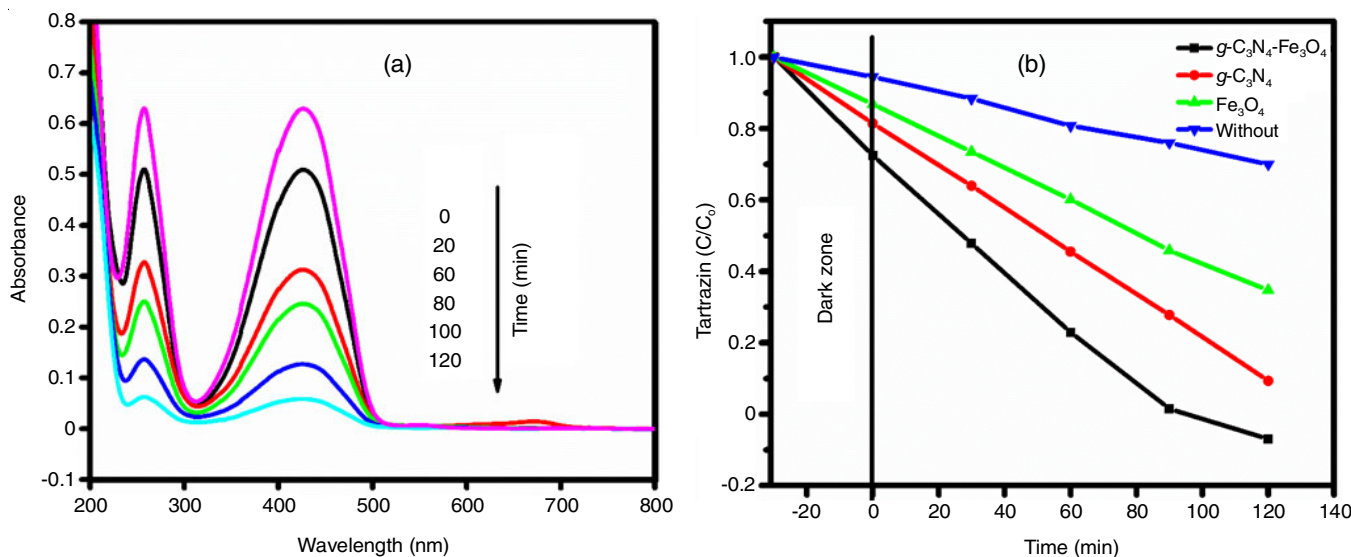
Fig. 6. Time dependent UV-vis spectral changes of tartrazine in the presence of under visible light irradiation (a) and photodegradation of tartrazine in the presence of Fe_3O_4, g-C_3N_4 and g-C_3N_4-Fe_3O_4 nanocomposites (b)
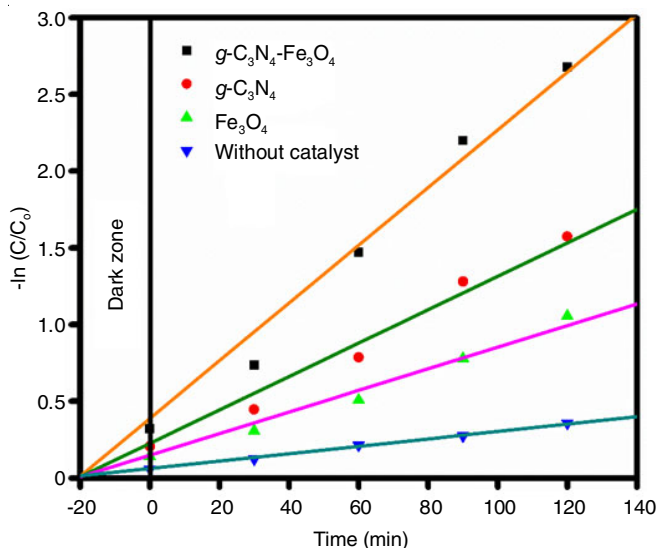
Fig. 7. Kinetic regime on the photodegradation of tartrazine in the presence of Fe_3O_4, g-C_3N_4 and g-C_3N_4-Fe_3O_4 nanocomposites

electrons of Fe_3O_4 will easily be transferred to the conduction band of g-C_3N_4 (wide band gap semiconductor). This leads to the electron-hole separation on the surface of the photocatalyst. The electrons react with surface adsorbed O_2 to produce $O_2^{\bullet-}$ and holes react with H_2O to create $^{\bullet}OH$. These reactive species enhance the degradation of tartazine [41].

Effect of g-C_3N_4/Fe_3O_4 dosage: The effect of catalyst on the photodegradation of tartrazine was analyzed by varying the concentration of g-C_3N_4-Fe_3O_4 from 0.05 g/L to 0.3 g/L for 20 µM tartrazine and the results are shown in Fig. 9. It exhibited the superior rate of degradation at g-C_3N_4-Fe_3O_4 concentration of 0.1 g/L. The rate of degradation was found to be increased with the increasing concentration of nanocomposites from 0.05 to 0.1 g/L. And the highest degradation (90%) occurred at 0.1 g/L. This is due to the surge in the availability of active sites at the surface of the catalyst. But a further increase in the catalyst concentration resulted in a decrease in the degradation rate. This may be attributed to the shielding of the penetrating light by the excessive amount of catalyst [42].
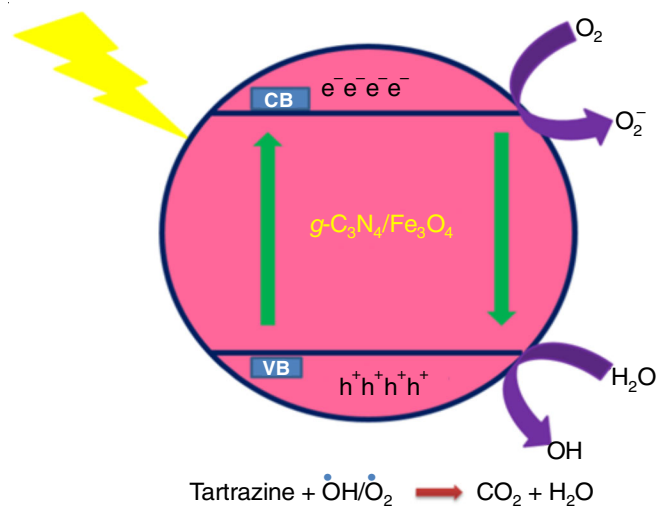

Fig. 8. Mechanism of tartrazine degradation by g-C_3N_4-Fe_3O_4

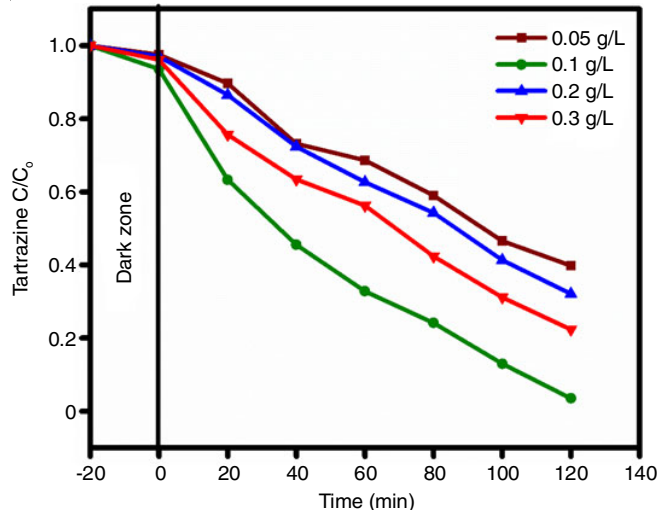Fig. 9. Effect of g-C_3N_4/Fe_3O_4 dosage on the photodegradation of tartrazine

Effect of initial tartrazine concentration: The influence of initial concentration of dye in the photodegradation process was analyzed by using various concentrations of dye ranging from 20 to 40 µM for the constant catalytic concentration of 0.1 g/L. Fig. 10 showed that as the rate of degradation is inversely proportional to the initial dye concentration. The highest degradation (90%) occurred at 20 µM tartrazine. This may be attributed to the reason that at higher dye concentrations, the generation of reactive oxygen species at the catalyst surface is reduced because of the hindrance created by the dye molecules against the photons, which doesn't allow them to react with the active sites at the catalyst surface.
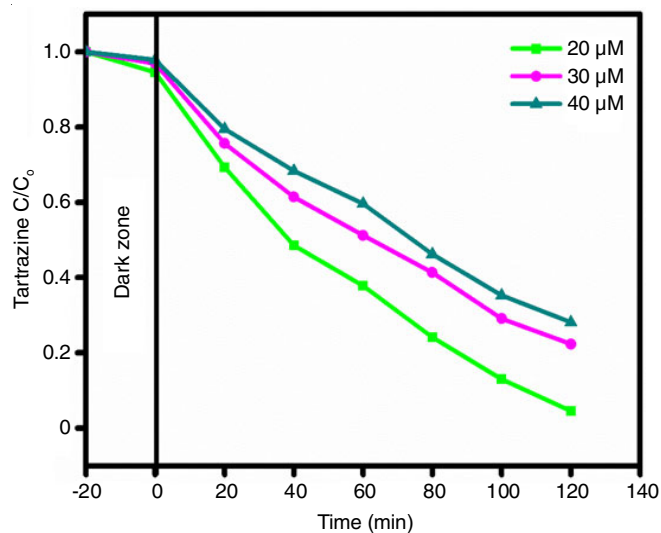

Fig. 10. Effect of initial concentration of tartrazine

Effect of pH: The effect of pH of solution on the photodegradation of tartrazine was studied by performing the reaction under various pH ranging from 3 to 8 for dye concentration 20 µM and catalyst dosage 0.1 g/L and the results are shown in Fig. 11. It was found that at lower pH, better photodegradation was happening and highest degradation (90%) was at pH = 3. As the pH increased from 3 to 8, the degradation percentage showed a decrease. The increased degradation in the lower pH may be attributed to the higher number of protons, which can protonate the reactive species and thereby enhance the adsorption of dye molecules on the catalyst surface. Tartrazine is an anionic dye, so more positive charge on the catalyst can enhance the adsorption of the dye molecules at the catalyst surface [15,42].

Conclusion

The *g*-C₃N₄/Fe₃O₄ nanocomposites were successfully synthesized by co-precipitation method as an efficient photocatalyst for the removal of tartrazine dye from aqueous solution. The as synthesized nanocomposite was characterized by various spectroscopic, analytical and morphological techniques. The *g*-C₃N₄/Fe₃O₄ nanocomposite was studied for the photodegradation of tartrazine dye in aqueous solution and displayed excellent results under the visible light irradiation compared with pure *g*-C₃N₄ and Fe₃O₄ nanoparticles. The optimum catalyst
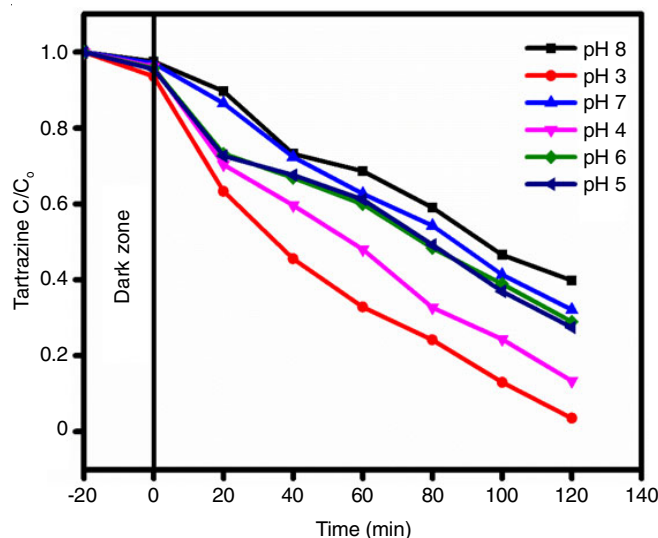

Fig. 11. Effect of pH on tartrazine degradation

loading for the highest degradation (90%) was observed as 0.1 g/L and the optimum initial concentration of dye as 20 µm in aqueous solution. The optimum pH for the photodegradation to happen was found to be pH 3. The kinetic study revealed that the photodegradation of tartrazine obeyed pseudo first-order kinetics.

CONFLICT OF INTEREST

The authors declare that there is no conflict of interests regarding the publication of this article.

REFERENCES

1. M. Wawrzkiewicz and Z. Hubicki, *J. Hazard. Mater.*, **164**, 502 (2009); https://doi.org/10.1016/j.jhazmat.2008.08.021
2. N. Arabzadeh, A. Khosravi, A. Mohammadi and N.M. Mahmoodi, *Desalination Water Treat.*, **57**, 3142 (2016); https://doi.org/10.1080/19443994.2014.989414
3. V.K. Gupta, R. Jain, A. Nayak, S. Agarwal and M. Shrivastava, *Mater. Sci. Eng. C*, **31**, 1062 (2011); https://doi.org/10.1016/j.msec.2011.03.006
4. H. Deng, J. Lu, G. Li, G. Zhang and X. Wang, *Chem. Eng. J.*, **172**, 326 (2011); https://doi.org/10.1016/j.cej.2011.06.013
5. H. Chen, *Curr. Protein Pept. Sci.*, **7**, 101 (2006); https://doi.org/10.2174/138920306776359786
6. D. Bilba, D. Suteu and T. Malutan, *Open Chem.*, **6**, 258 (2008); https://doi.org/10.2478/s11532-008-0019-2
7. H. Jiang, P. Chen, S. Luo, X. Tu, Q. Cao and M. Shu, *Appl. Surf. Sci.*, **284**, 942 (2013); https://doi.org/10.1016/j.apsusc.2013.04.013
8. R. Gong, X. Zhang, H. Liu, Y. Sun and B. Liu, *Bioresour. Technol.*, **98**, 1319 (2007); https://doi.org/10.1016/j.biortech.2006.04.034
9. N. Dizge, C. Aydiner, E. Demirbas, M. Kobya and S. Kara, *J. Hazard. Mater.*, **150**, 737 (2008); https://doi.org/10.1016/j.jhazmat.2007.05.027
10. A. Mittal, L. Kurup and J. Mittal, *J. Hazard. Mater.*, **146**, 243 (2007); https://doi.org/10.1016/j.jhazmat.2006.12.012
11. P. Ratna, *Int. J. Environ. Sci.*, **3**, 940 (2012).
12. C. Klett, A. Barry, I. Balti, P. Lelli, F. Schoenstein and N. Jouini, *J. Environ. Chem. Eng.*, **2**, 914 (2014); https://doi.org/10.1016/j.jece.2014.03.001
13. M.-S. Li, Z.-P. Zhao and M.-X. Wang, *Chem. Eng. J.*, **259**, 53 (2015); https://doi.org/10.1016/j.ces.2014.09.015

14. E. Akhondi, B. Wu, S. Sun, B. Marxer, W. Lim, J. Gu, M. Burkhardt, L. Liu, D. McDougald, W. Pronk and A.G. Fane, *Water Res.*, **70**, 158 (2015);
https://doi.org/10.1016/j.watres.2014.12.001

15. Y. Zhou, Y. Qin, W. Dai and X. Luo, *ACS Omega*, **4**, 546 (2019);
https://doi.org/10.1021/acsomega.8b03267

16. F.C. Moreira, R.A.R. Boaventura, E. Brillas and V.J.P. Vilar, *Appl. Catal. B: Environ.*, **202**, 217 (2017);
https://doi.org/10.1016/j.apcatb.2016.08.037

17. I.P.A.F. Souza, L.H.S. Crespo, L. Spessato, S.A.R. Melo, A.F. Martins, A.L. Cazetta and V.C. Almeida, *J. Environ. Chem. Eng.*, **9**, 104753 (2021);
https://doi.org/10.1016/j.jece.2020.104753

18. W. Sangchay, *J. Nanotechnol.*, **2017**, 7902930 (2017);
https://doi.org/10.1155/2017/7902930

19. A. Aleboyeh, M.B. Kasiri, M.E. Olya and H. Aleboyeh, *Dyes Pigments*, **77**, 288 (2008);
https://doi.org/10.1016/j.dyepig.2007.05.014

20. W. Wang, M.O. Tadé and Z. Shao, *Chem. Soc. Rev.*, **44**, 5371 (2015);
https://doi.org/10.1039/C5CS00113G

21. C. Chen, W. Ma and J. Zhao, *Chem. Soc. Rev.*, **39**, 4206 (2010);
https://doi.org/10.1039/b921692h

22. J. Zhu, S. Wei, H. Gu, S.B. Rapole, Q. Wang, N. Haldolaarachchige, Z. Luo, D.P. Young and Z. Guo, *Environ. Sci. Technol.*, **46**, 977 (2012);
https://doi.org/10.1021/es2014133

23. L. Huang, H. Xu, Y. Li, H. Li, X. Cheng, J. Xia, Y. Xu and G. Cai, *Dalton Trans.*, **42**, 8606 (2013);
https://doi.org/10.1039/c3dt00115f

24. H. Li, J. Liu, W. Hou, N. Du, R. Zhang and X. Tao, *Appl. Catal. B*, **160-161**, 89 (2014);
https://doi.org/10.1016/j.apcatb.2014.05.019

25. S. Kamal, S. Balu, S. Palanisamy, K. Uma, V. Velusamy and T.C.K. Yang, *Results in Physics*, **12**, 1238 (2019);
https://doi.org/10.1016/j.rinp.2019.01.004

26. W. Guo, K. Fan, J. Zhang and C. Xu, *Appl. Surf. Sci.*, **447**, 125 (2018);
https://doi.org/10.1016/j.apsusc.2018.03.080

27. S.G. Kumar and L.G. Devi, *J. Phys. Chem. A*, **115**, 13211 (2011);
https://doi.org/10.1021/jp204364a

28. S. Zhang, P. Gu, R. Ma, C. Luo, T. Wen, G. Zhao, W. Cheng and X. Wang, *Catal. Today*, **335**, 65 (2019);
https://doi.org/10.1016/j.cattod.2018.09.013

29. B. Rhimi, C. Wang and D. Bahnemann, *J. Phys. Energy*, **2**, 042003 (2020);
https://doi.org/10.1088/2515-7655/abb782

30. Y. Fu, T. Huang, L. Zhang, J. Zhu and X. Wang, *Nanoscale*, **7**, 13723 (2015);
https://doi.org/10.1039/C5NR03260A

31. X. Wang, K. Maeda, A. Thomas, K. Takanabe, G. Xin, J.M. Carlsson, K. Domen and M. Antonietti, *Nat. Mater.*, **8**, 76 (2009);
https://doi.org/10.1038/nmat2317

32. B. Zhu, P. Xia, Y. Li, W. Ho and J. Yu, *Appl. Surf. Sci.*, **391**, 175 (2017);
https://doi.org/10.1016/j.apsusc.2016.07.104

33. L. Yang, J. Tian, J. Meng, R. Zhao, C. Li, J. Ma and T. Jin, *Molecules*, **23**, 562 (2018);
https://doi.org/10.3390/molecules23030562

34. L. Liu, Y. Qi, J. Hu, Y. Liang and W. Cui, *Appl. Surf. Sci.*, **351**, 1146 (2015);
https://doi.org/10.1016/j.apsusc.2015.06.119

35. M. Rajabi, K. Mahanpoor and O. Moradi, *Composites B Eng.*, **167**, 544 (2019);
https://doi.org/10.1016/j.compositesb.2019.03.030

36. Y. Wang, X. Wang and M. Antonietti, *Angew. Chem. Int. Ed.*, **51**, 68 (2012);
https://doi.org/10.1002/anie.201101182

37. Y. Yao, Y. Cai, F. Lu, J. Qin, F. Wei, C. Xu and S. Wang, *Ind. Eng. Chem. Res.*, **53**, 17294 (2014);
https://doi.org/10.1021/ie503437z

38. P. Makula, M. Pacia and W. Macyk, *J. Phys. Chem. Lett.*, **9**, 6814 (2018);
https://doi.org/10.1021/acs.jpclett.8b02892

39. K. Vignesh, M. Rajarajan and A. Suganthi, *J. Ind. Eng. Chem.*, **20**, 3826 (2014);
https://doi.org/10.1016/j.jiec.2013.12.086

40. K. Vignesh, A. Suganthi, B.-K. Min, M. Rajarajan and M. Kang, *RSC Adv.*, **5**, 576 (2015);
https://doi.org/10.1039/C4RA14291H

41. K. Vignesh, R. Hariharan, M. Rajarajan and A. Suganthi, *Mater. Sci. Semiconductor Process.*, **16**, 1521 (2013);
https://doi.org/10.1016/j.mssp.2013.04.025

42. P. Bansal and D. Sud, *Desalination*, **267**, 244 (2011);
https://doi.org/10.1016/j.desal.2010.09.034